Nano Research Energy

ISSN 2791-0091 (print); 2790-8119 (online)
https://doi.org/10.26599/NRE.2024.9120139

Research Article

All-cellulose triboelectric textile with complete biodegradability for eco-friendly smart wearable electronics

Qiru Lian, Jiaxin Li, Ting Li, Qiuyu Li, Yifang Liang, Hanguang Wu (✉), and Rui Wang

Beijing Key Laboratory of Clothing Materials R & D and Assessment, Beijing Institute of Fashion Technology, Beijing 100029, China

Received: 7 May 2024 / **Revised:** 5 August 2024 / **Accepted:** 2 September 2024

ABSTRACT

The booming of the triboelectric textiles (TENG-Ts) in recent years is accompanied with the e-waste crisis and a huge hidden danger to the natural environment, thus it is highly desired to create the eco-friendly TENG-Ts with degradability for the sustainable development of the smart textiles. In this study, we fabricated a regenerated cellulose-based TENG-T (RC TENG-T) with complete biodegradability through braiding and knitting technology, in which two friction layers were chemically modified by using two silane hydrolysates with opposite electro-affinity. The energy harvesting ability of the RC TENG-T was significantly improved, and the open-circuit voltages (V_{OC}) and short-circuit current (I_{SC}) were enhanced to nearly 9.8 V and 160 nA respectively. The RC TENG-T can be completely bio-degraded under the function of cellulase after 72 h, endowing it with wide application potential as eco-friendly smart wearable devices including microelectronics power source and self-powered sensor with capability of monitoring human physical conditions and the external pressure.

KEYWORDS

triboelectric nanogenerator, smart textile, cellulose, biodegradability, self-powered

1 Introduction

Over the past decade, wearable electronics have attracted comprehensive attention and developed rapidly because of their large application potential in healthcare monitoring, human-machine interfaces, and artificial intelligence technology [1–3]. In practical applications, it is highly desirable to exploit wearable electronics which do not need external power sources to improve the portability, comfortability, and serving life of the device, and the development of the flexible triboelectric nanogenerators (TENGs) provides a new strategy for the self-powered wearable electronics [4–7]. Currently, most flexible TENGs are fabricated by using polymers with high electron affinity including polyethyleneimine (PEI), polydimethylsiloxane (PDMS), and various fluoropolymers, to form the triboelectric layers to enhance the energy harvesting capability [5, 8–10]. The strong chemical stability and non-degradability of these polymers lead to the difficulties in recycling and degradation of the TENGs, leading to a large amount of e-waste that poses a huge hidden danger to the natural environment and ecological balance. Therefore, the fabrication of the eco-friendly and completely bio-degradable TENGs is crucial for the sustainable development of this new energy strategy [11–13].

Tremendous efforts have been made to utilize the natural polymers into the TENGs to improve their biodegradability, in which cellulose has attracted wide attention due to its abundant resource and high biocompatibility [12, 14, 15]. As a typical bio-degradable polymer, cellulose provides the sustainable development route of flexible TENGs that can come from nature and go back to nature [14, 16]. A large part of cellulose-based flexible TENGs applied the cellulose materials as the substrate, onto which the electrode layers and friction layers were subsequently formed by using the conductive materials and the triboelectric materials respectively [17–20]. In some other work, the cellulose materials are also used in the construction of the triboelectric-generating outer layer in TENGs due to its slight positron affinity [21–23]. Kim fabricated an allicin-grafted cellulose nanofiber film containing square micropatterns on the surface, and successfully used it as the tribo-positive material to enhance the triboelectric output performance of the cellulose-based TENGs with polyvinylidene fluoride (PVDF) film as the tribo-negative material [24]. Guo developed a high-output flexible TENG by using porous cellulose acetate/PEI biocomposite as the tribo-positive material [25]. In Cheng's work, they fabricated a cellulose-based TENG with the cyanoethyl cellulose/PVDF membrane as the tribo-negative layer [26]. Pan prepared a cellulose II aerogel via a dissolution-regeneration process, and used it to fabricate a TENG with polytetrafluoroethylene (PTFE) as the tribo-negative material [27]. Guo developed a porous nanocomposite fabric by incorporating nano-Al_2O_3 fillers into cellulose acetate networks, and used it as the tribo-positive material to form a TENG, in which the silicone rubber was used as the tribo-negative material [28]. Wei fabricated an all-fiber-structured TENG by electrospinning, in which the ethyl

Address correspondence to Hanguang Wu, hanguangwu@bift.edu.cn

cellulose/polyamide nanofiber mats constructed the tribo-positive material and the MXene-based PVDF nanofiber mats constructed the tribo-negative material [29]. It can be concluded that the cellulose is seldom solely used as the triboelectric material of TENGs due to its weak electronegativity, and the non-degradable materials (eg., PTFE, PVDF, PEI, silicone rubber, etc.) with high tribo-electrification are always inevasible in the flexible TENGs fabrication to guarantee their high triboelectric output, leading to the inevitable pollution to the environment. Some effort has been made for developing the all-cellulose TENGs simultaneously exhibiting complete bio-degradability and ideal triboelectric performances [30, 31]. Zhang successfully prepared an all-cellulose TENG with the ultrahigh power density of 307 $W \cdot m^{-2}$ by using regenerated cellulose and commercial cellophane as the tribo-layers, as well as graphite foils as the electrodes [30], but the high modulus of the triboelectric materials and the intensive film structure of the TENG resulted in its inferior flexibility and comfortability, thereby limiting its application as smart wearable electronics. Yang developed an all-cellulose TENG with sandwich structure, in which the bacterial cellulose (BC) membrane and the conductive BC/carbon nanotubes/polypyrrole membrane are used to form the triboelectric layers [31]. Nowadays, majority of the cellulose-based TENGs appear in planar structures (such as film and strip structure) with high integration difficulty and low human motions adaptation, thus reducing their capability to meet the requirements to form the portable and wearable electronics [30–35]. The triboelectric textiles (TENG-Ts), as a typical TENG combining the characteristics of textiles (eg., breathability, washability, flexibility, lightweight, etc.), and the energy harvesting and sensing capability of TENGs, providing a versatile solution for future portable, flexible, and green energy supply in wearable systems [36–38]. However, the cellulose-based TENG-Ts fabricated by simple and continuous weaving technique is seldom developed despite of its advantages including wearing comfortability and large-scale production.

In this study, we fabricated an all-cellulose TENG-T by braiding and knitting technology, during which process two friction layers formed by regenerated cellulose (RC) yarns are chemically modified by using two silane hydrolysates with opposite electro-affinity and thus significantly improved the energy harvesting ability of the obtained regenerated cellulose-based TENG-T (RC TENG-T). We aim to develop a simple and continuous fabrication process for a complete bio-degradable e-textile for eco-friendly energy resources and self-powered smart wearable sensor.

2 Experimental

Preparation of the AgNPs-coated RC yarn: First, the commercially available bamboo viscose yarn was used as the raw regenerated cellulose yarn (150D, Kunlunjie Co., Ltd., China) in this study, which was soaked in ethanol and ultrasonicated for 15 min (400 W) for pretreatment, and then put into the dopamine solution (0.3 wt.%) at pH=8.5 and reacted at room temperature for 24 h. The dopamine-treated RC yarns were subsequently put into 1.4 wt.% $AgNO_3$ solution, and then added 2.5 wt.% glucose solution and reacted at room temperature for 2 h. The silver nanoparticles (AgNPs) were uniformly and tightly attached on the inner and outer sides of the yarns to obtain the AgNPs-coated RC yarns with good electrical conductivity.

Chemical modification of the RC yarn: The polarity of RC yarn was enhanced by surface modification by AEAPDMS or PFOTES [39, 40]. AEAPDMS modification was performed on RC yarn by immersing the RC yarns into the silane hydrolysate with 10/80/20 (*v*/*v*/*v*) AEAPDMS, ethanol, and water under 5 min (400 W) ultrasonication, then the RC yarns were heat-treated at 120 °C for 13 h, and the AEAPDMS modified RC yarns were obtained after washing and drying. PFOTES modification was performed on RC yarn by immersing the RC yarns into the silane hydrolysate with 10/80/20 (*v*/*v*/*v*) PFOTES, ethanol, and water under the 80 °C water bath for 6 h, and the PFOTES modified RC yarns were obtained after rinsing and drying.

Fabrication of RC TENG-T: Two composite yarns were fabricated by tightly braiding AEAPDMS modified RC yarns or PFOTES modified RC yarns onto the AgNPs-coated RC yarn on a high-speed braiding machine (XD95-8D-4T, Jiangsu Xiangdao Precision Machinery Co., Ltd., China) [38]. Then, these two yarns were woven into a scuba knitting fabric with a separately bi-layered structure by using semiautomatic hand-flat knitting machine (2000, Guosheng Knitting Machinery Factory, China). The conductive cores in the composite yarns functions as the electrodes for the charge transferring, thus an all-cellulose TENG-T (RC TENG-T) with two-electrode mode was obtained for subsequent characterization and application. In addition, the all-cellulose TENG-Ts with the unmodified RC yarns as one triboelectric layer were also fabricated in the same method for comparison.

Measurement and characterization: Scanning electron micrographs (SEM) were recorded using a Sirion 200 field-emission scanning electron microscope (FEI, USA) at an accelerating voltage of 10 kV. The conductivity was recorded by using electrochemical workstation (CHI440A, Chenhua Instruments Co., Ltd., China). Fourier-transform infrared spectroscopy (FTIR, VERTES 70, Germany) was used to detect the functional groups on the RC yarns before and after chemical modification, and the range was from 4000–400 cm^{-1}. The crystallinity was measured by using X-ray diffraction (XRD, SMARTLAB 3KW, Japan), and the scanning range was 2θ = 5°–50° with the scanning speed of 5 °·min^{-1}. The tensile properties of the original RC yarn and the chemically modified RC yarns were measured by using a tensile apparatus (TSE202A, Shenzhen Wance Testing Machine Co., Ltd., China) at a crosshead speed of 200 mm·min^{-1}. The hydrophobicity of the fabric layers was analyzed by using contact angle tester (DSA100, Germany).

The surface potentials of the RC yarns before and after chemical modification were determined using an electrostatic voltmeter (TREK 542A-2, USA). A dielectric spectrometer (Concept 50, German) was used to characterize the dielectric constant of the RC yarns before and after chemical modification. A programmable electrometer (Keithley 6514) was used for the electrical output and surface charge density measurement, and the periodic contact-separation motions were applied by a linear motor. The washability test of the RC TENG-T was conducted according to the mainstream simulation washing method previously reported [38, 41, 42]. The air resistance value of RC TENG-T was tested with a piece of fabric (20 cm^2) under 100 Pa pressure by an air permeability instrument (YG461E) according to the standard (GB/T 5453-1997). A 25×25×25 cm^3 closed box is used to create different humidity environments for testing the triboelectric performances in the different humidity environments. The RC TENG-T, a hygrometer, and a humidifier are placed in the box. Humidify the humidifier for a period of time. When the humidity in the box reaches the predetermined humidity (60%, 70%, 80%, 90% and 99% RH), turn off the humidifier and test the triboelectric output of the RC TENG-T. The biodegradability of RC TENG-T was performed in a 3:2 (*v*/*v*) HAc-NaAc buffer (pH=4.8) with 0.5 wt.% 1,4-(1,3:1,4)-β-D-Glucan 4-

glucanohydrolase under 50 °C, and the sample was taken out every 12 hours for the morphology observation and weight measurement.

During the application test of the RC TENG-T as a power supply equipment, the RC TENG-T was integrated with a commercial capacitor (33 μF) to drive an electronic watch. During the application test of the RC TENG-T as a self-powered pressure sensor, the fabric was fixed at heel, finger joint, and arm to monitor different human motions. In addition, an intelligent Taekwondo scoring system was constructed through connecting RC TENG-T with signal processing/transmission module and electric displaying device. The signal processing/transmission module consists of amplifier, microcontroller unit, and relay, which magnify, analyze and further transmit the electrical signals from RC TENG-T.

3 Results and discussion

The RC TENG-T in this study is fabricated solely by using the RC yarns from the natural plants including bamboo, leaf, and cotton, thus presenting high eco-friendliness and sustainability (see Fig. 1(a)). Through braiding and knitting technique, a bi-layered textile with two types of chemically modified RC yarns as two friction layers is formed. The chemical modification is desired to introduce amino groups or fluorine-containing functional groups onto the friction layers, thus improving the tribo-electric output of the obtained RC TENG-T and endowing it with wide application potential in smart wearable electronics (such as energy harvesting, human motion monitoring, and human-machine interaction) coupled with its advanced flexibility and comfortability. The natural resources of RC TENG-T provide it with good biodegradability after the usage, thereby meeting the urgent requirements for both energy production and emission reduction. In addition, the application of high-braiding machine and hand-flat knitting machine for the RC TENG-Ts production in this work provides the possibility for the large-scale production of the high performed smart textiles based on RC.

Figure 1(b) shows the photograph of a RC TENG-T, indicating the separate upper and bottom fabric layers and the space formed between them. The knitted structure constructed in two fabric layers of the RC TENG-T (as shown in Fig. 1(c)) provides it with high stretchability to guarantee its deformation consistency with the human body during its wearable usage. The RC-based composite yarns used for knitting are prepared by tightly braiding EAPDMS modified RC yarns (RC-NH_3) or PFOTES modified RC yarns (RC-F) onto the silver nanoparticles (AgNPs)-coated RC yarns (see Figs. 1(d) and 1(e)). The AgNPs-coated RC yarn, functioning as the core electrode of the TENG-T, is fabricated by silver mirror reaction, during which process the AgNPs were formed and then uniformly and tightly attached on the inner and outer sides of the RC yarn (see Fig. S1(a) in the Electronic Supplementary Material (ESM)). The concentration of $AgNO_3$ solution is optimized as 0.08 M to maximize the electrical conductivity of the AgNPs-coated RC yarn (see Fig. S1(b) in the ESM). The dopamine treatment of RC yarn before AgNPs coating results in the formation of a uniform adhesive layer upon the RC surface (see Fig. S2(a) in the ESM), which is the key to the tight attachment of the AgNPs and the conductivity improvement of the AgNPs-coated RC yarn (see Fig. S2(b) in the ESM). Figures 1(f) and 1(g) respectively show the surfaces of the RC-NH_3 and the RC-F. The chemically modified RC yarns present rough surface compared with the unmodified RC yarn (as shown in Fig.

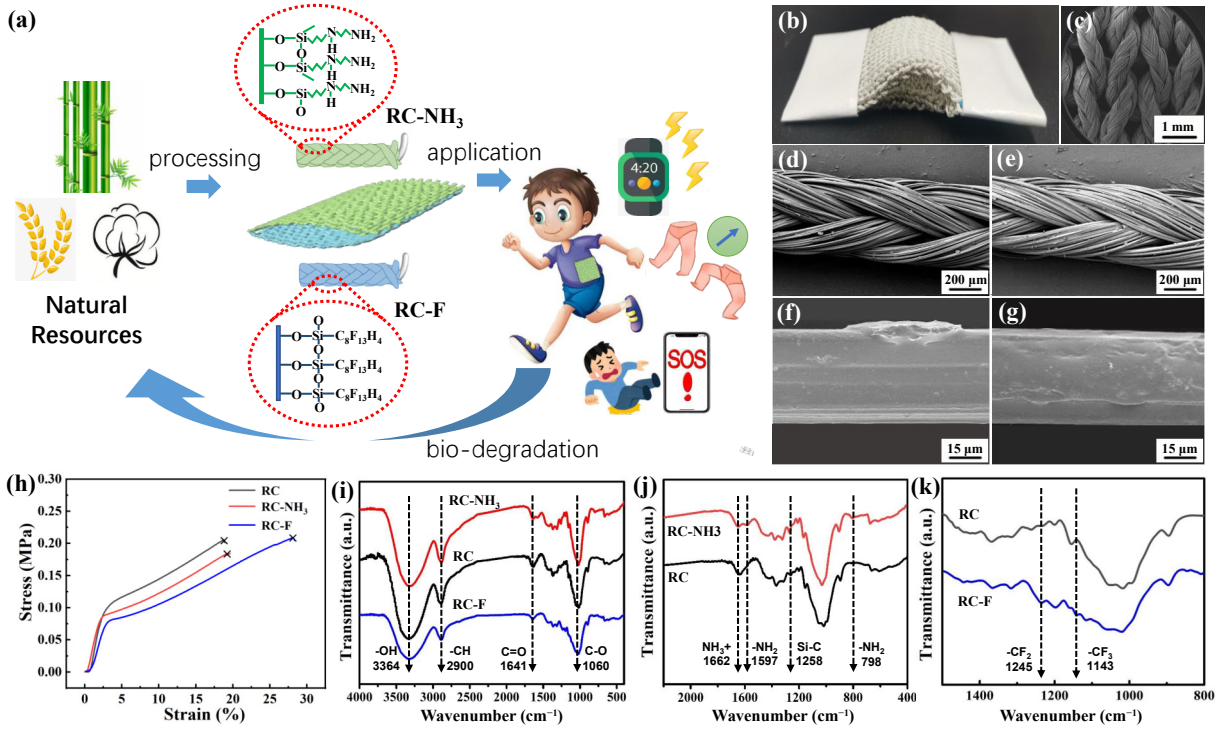

Figure 1 (a) Circulation of RC TENG-T from natural resources to application. (b) Photograph of a RC TENG-T with separately bi-layered structure. (c) SEM image of knitted structure in the fabric layers of the RC TENG-T. (d) SEM image of the RC-based composite yarns with EAPDMS modified RC yarns (RC-NH_3) as sheath layer. (e) SEM image of the RC-based composite yarns with PFOTES modified RC yarns (RC-F) as sheath layer. (f) SEM image of EAPDMS modified RC yarn (RC-NH_3). (g) SEM image of PFOTES modified RC yarn (RC-F). (h) Stress-strain curves of the RC yarns before and after chemical modification. (i) FT-IR of the RC yarns before and after chemical modification at 4000–400 cm^{-1}. (j) FT-IR of RC yarns before and after AEAPDMS modification at 2200–400 cm^{-1}. (k) FT-IR of RC yarns before and after PFOTES modification at 1500–800 cm^{-1}.

S3 in the ESM), indicating the roughening effect of the chemical modification on RC yarn. However, the basic morphology of RC yarn was not destroyed, and the original features of the RC yarn were retained after the chemical modification by AEAPDMS or PFOTES, thus the mechanical properties of RC-NH_3 and RC-F are comparable with those of the unmodified RC yarn (Fig. 1(h)).

FT-IR was used to characterize the functional groups on the surface of the friction layers and evaluate the chemical modification degree of the RC yarns. Figure 1(i) shows FT-IR spectra of RC yarns before and after chemical modification by AEAPDMS or PFOTES. It can be seen that most of the typical peaks of RC retain after modification. For example, wide absorption peaks appear at 3364 and 2900 cm^{-1}, which are attributed to O-H and C-H stretching respectively. The absorption peak at 1641 cm^{-1} is due to the carboxyl group and at 1060 cm^{-1} is attributed to C-O stretching within the aliphatic hydroxyl of the RC yarn. In addition, the absorption peaks at 1100–1000 cm^{-1} are attributed to the typical peaks of Si-O-Si and Si-O-C, which are covered by some typical peaks of the RC yarn. After the AEAPDMS modification, new typical peaks appeared at 2300–400 cm^{-1} (see Fig. 1(j)), including the peaks at 1662, 1597, 1258, and 798 cm^{-1}. The absorption peak for a water molecule at 1638 cm^{-1} red-shifted to 1662 cm^{-1}, which was assigned to the aminosilane and was associated with asymmetric NH_3^+ deformation that formed via the interaction of primary amines with water or silanol groups. The emergence of new peaks at 1597 and 798 cm^{-1} are attributed to -NH_2 bending and -NH_2 wagging, respectively. Additionally, the high-intensity peak of Si-CH_3 at 1258 cm^{-1} was also observed in the FT-IR spectrum of RC-NH_3. The results preliminarily confirmed the successful AEAPDMS modification of the RC yarn with amino groups grafted onto its surface. Figure 1(k) shows the FT-IR spectra of RC yarns before and after PFOTES modification at wavelength of 1500–800 cm^{-1}. It can be seen that two new peaks appear at 1245 and 1143 cm^{-1} in the FT-IR spectrum of RC-F, corresponding to characteristic stretching vibrations for -CF_2 and -CF_3 respectively. According to the previous reports, it can be speculated from the FT-IR spectra that the RC yarns have been successfully modified with AEAPDMS or PFOTES. In addition, XRD was also used to evaluate the effect of the surface modification on the RC-based friction layers. XRD patterns of RC yarns before and after AEAPDMS and PFOTES modification are shown in Fig. S4 in the ESM. After the chemical modification by AEAPDMS or PFOTES, the obtained RC-NH_3 and RC-F both retained the diffraction peaks of cellulose II [40, 43], consistent with the FI-IR results. However, the peak intensity was weaker for the RC-NH_3 and RC-F compared to that of unmodified RC yarn, indicating the crystallinity deterioration effect of AEAPDMS or PFOTES modification on RC yarn. This should be attributed to the slight degradation of the crystalline zone in RC yarn after chemical modification, during which process the hydroxyl groups were partly replaced by amorphous aminosilane chains or fluorosilane chains [39, 40]. The hydrophilic and hydrophobic properties of the RC yarns before and after chemical modification were also evaluated by using contact angle measurements, and the results are shown in Fig. S5 in the ESM. The water droplet is absorbed promptly (0.08 s) when it contacts with the unmodified RC textile due to the super hydrophilicity and the porous structure of the textile (see Fig. S5(a) in the ESM). After the AEAPDMS or PFOTES modification, the RC-based textile can stably sustain a water droplet during a much longer period, indicating the significant hydrophobicity enhancement of the modified textile. The contact angle of the textile with the RC-NH_3 sheath layer keeps almost unchanged around 118° in 120 s (Fig. S5(b) in the ESM), and the textile with the RC-F sheath layer presents the highest contact angle of 121°, which keeps unchanged even after 240 s (Fig. S5(c) in the ESM). The significant hydrophobicity enhancement of the textile also proves the successful modification of the RC yarns, which is in consistent with the FI-IR and XRD results.

The chemical modification is desired to form two RC-based friction layers with opposite charge affinities in RC TENG-T and thus improving its triboelectric output under the function of pressure. In order to study the effect of the chemical modification of the RC sheath layer on the triboelectric output of RC TENG-T, we fabricated two RC-based TENG-T comparative samples, in which one triboelectric fabric layer was woven by using the composite yarns with unmodified RC sheath layer. The energy generating capability of RC TENG-T is characterized through measuring the open-circuit voltage (V_{OC}), short-circuit current (I_{SC}), and short-circuit charge transfer (Q_{SC}) under a periodic compressing force of 60 N at frequency of 2 Hz, and the results are shown in Figs. 2(a)–2(c). The RC TENG-T with two chemically modified RC sheath layers exhibits a much higher triboelectric output compared with two RC-based TENG-T comparative samples, and the V_{OC}, I_{SC}, and Q_{SC} reach approximately 9.8 V, 160 nA, and 5.8 nC, respectively.

The detailed working mechanism of the RC TENG-T is schematically shown in Fig. S6 in the ESM. The composite yarns with RC-NH_3 as the sheath layer were woven into the positive triboelectric fabric, and the composite yarns with RC-F as the sheath layer were woven into the negative triboelectric fabric. No charge is generated when there is no contact between two triboelectric fabric layers in the original position. When an external pressure brings the friction surface of the positive triboelectric fabric and negative triboelectric fabric into physical contact, two chemically modified RC sheath layers are charged (see Fig. S6-I in the ESM). Once the external force is removed, electrons transfer between two electrodes in RC TENG-T to keep the electric neutrality in the positive triboelectric fabric layer and the negative triboelectric fabric layer, thus leading to the potential change and the current flow in the external circuit (Fig. S6-ii in the ESM). The electrons flow from the AgNPs-coated RC yarn electrode encapsulated by the RC-F to the AgNPs-coated RC yarn electrode encapsulated by the RC-NH_3 (see the insets in Fig. S6 in the ESM), causing the higher electric potential of the electrode encapsulated by the RC-F. Therefore, the RC-F and RC-NH_3 are deduced to be charged negatively and positively respectively, indicating the higher electron affinity of the RC-F. When two fabric layers are separated far enough, the transferring of the electrons is terminated to keep an equilibrium state (Fig. S6-iii in the ESM). When the positive triboelectric fabric approaches the negative triboelectric fabric again, electrons flow from the AgNPs-coated RC yarn electrode encapsulated by the RC-NH_3 to the AgNPs-coated RC yarn electrode encapsulated by the RC-F, producing a reversed current (Fig. S6-iv in the ESM). Therefore, AC signals are generated due to the periodic contact and separation of the upper and bottom fabric layers in RC TENG-T. From the triboelectric mechanism of the RC TENG-T, it can be seen that the output performance of the RC TENG-T directly depends on the surface charge density (σ) of the friction materials. In addition, as previously reported, the output performance of TENG can also be significantly improved by increasing the dielectric constant (ε_r) of the friction materials [44–46]. The σ (Fig.

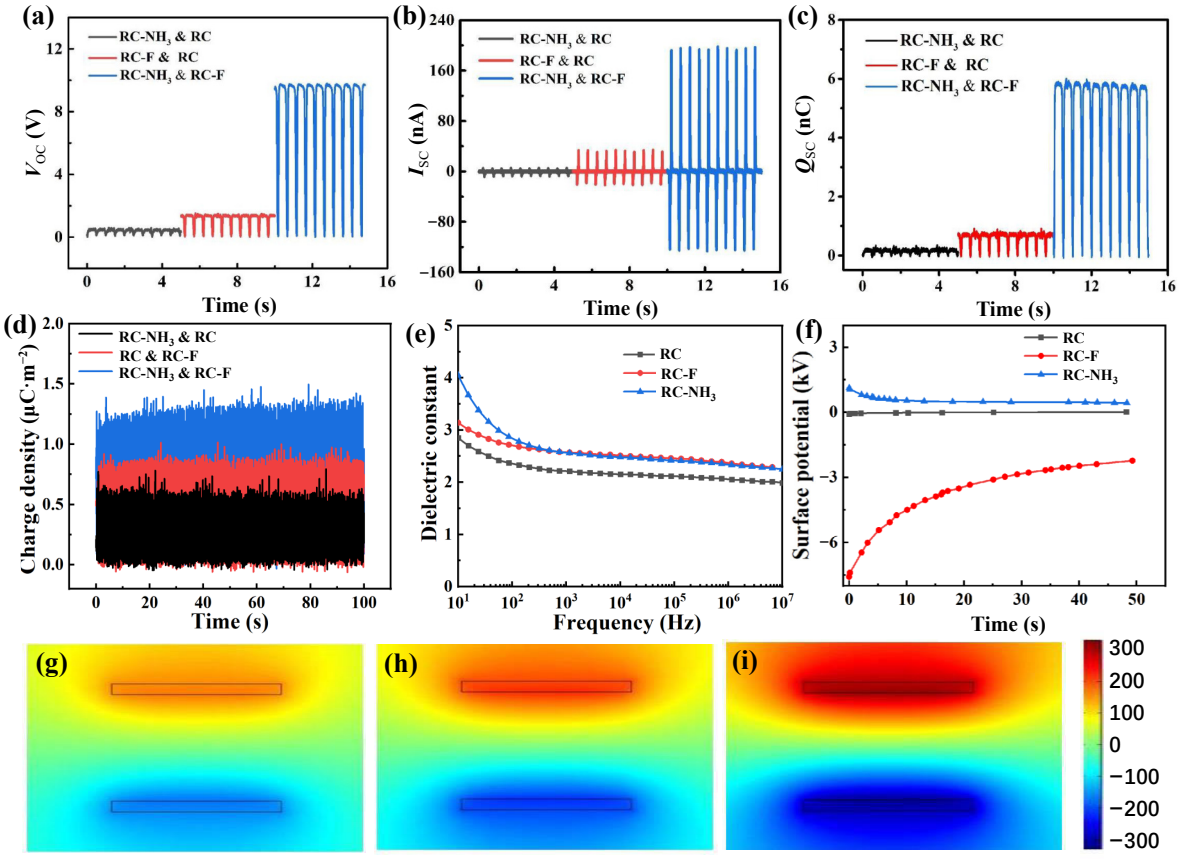

Figure 2 (a) the open-circuit voltage (V_{OC}), (b) short-circuit current (I_{SC}), and (c) short-circuit charge transfer (Q_{SC}) of the RC TENG-T and two RC-based TENG-T comparative samples with one unmodified RC friction layer (under the compressing force of 60 N and the frequency of 2 Hz). (d) The charge density of the RC yarns before and after chemical modification. (e) The dielectric constant of the RC yarns before and after chemical modification. (f) The surface potential of the RC yarns before and after chemical modification. COMSOL simulation for electrical potential in the (g) RC-based TENG-T with one unmodified RC sheath layer and one RC-NH_3 sheath layer; (h) RC-based TENG-T with one unmodified RC sheath layer and one RC-F sheath layer; (i) RC-based TENG-T with two chemically modified RC sheath layers.

2(d)) and ε_r (Fig. 2(e)) of unmodified RC, RC-NH_3, and RC-F were tested and compared respectively, indicating the charge density improvement effect and dielectric properties improvement effect of chemical modification on RC yarns, thus revealing the reason for the much higher output performance of the RC TENG-T with two chemically modified fabric layers. The surface potential difference between two friction layers in the RC-based TENG-T is also enhanced after chemical modification (as shown in Fig. 2(f)), leading to the electrons escape capability between contact surfaces [47]. To further elucidate the effect of the chemical modification on the output performance of RC TENG-T, the potential distribution of three RC-based TENG-T samples was simulated by using COMSOL multi-physics software, as presented in Figs. 2(g)–2(i)). Under the conditions of same separation distance and contact area, the simulated potential distribution of the RC TENG-T with two chemically modified RC sheath layers is much higher than those of two RC-based TENG-T comparative samples, which is consistent with the experimental results shown in Fig. 2(a).

In order to further investigate the energy harvesting performances of the RC TENG-T, the V_{OC}, I_{SC}, and Q_{SC} values at different tapping frequencies ranging from 1 to 5 Hz are tested, and the compressing force is fixed at 60 N (see Fig. 3(a) and Fig. S7 in the ESM). Both V_{OC} and Q_{SC} keep unchanged with the increase of frequency, but the I_{SC} increases obviously from 50 to 390 nA with the increased tapping frequency from 1 to 5 Hz (see Fig. S7(a) in the ESM) due to the increased charge flow rate at high frequency [48]. The V_{OC} of the RC TENG-T under different applied compression is shown in Fig. 3(b), indicating the enhanced energy harvesting capability of the textile under the increased pressure caused by the enlarged friction area. The V_{OC}-pressure curve can be divided into three zones according to the different curve slopes, which is defined as the sensitivity of the RC TENG-T while the textile is used as a self-powered pressure sensing device [49]. The RC TENG-T shows the highest sensitivity of 1.25 V·N^{-1} at low pressure below 5 N, and the pressure sensitivity decreases significantly to 0.14 V·N^{-1} in the medium-pressure region of 5–35 N. When the pressure is higher than 35 N, the sensitivity is as low as 0.045 V·N^{-1}. The deterioration of the pressure sensitivity of RC TENG-T with the increased pressure should be mainly attributed to the gradual saturation of the effective friction area under the function of large pressure [38, 50]. When different external load resistances (R) are connected with RC TENG-T, the variation of output current (I) and power density (W) of the RC TENG-T is characterized, which are shown in Fig. 3(c). Under the tapping frequency of 2 Hz, I shows almost no change when the load resistance is below 0.1 MΩ, but decreases subsequently as the load resistance increases from 0.1 MΩ to 1 GΩ. The W can be calculated by:

$$W = \frac{I^2 \cdot R}{A} \quad (1)$$

where A is the effective area. The maximum W of RC TENG-T is 12.9 mW·m^{-2} at a load resistance of 400 MΩ.

The stability of the RC TENG-T is tested by continuously

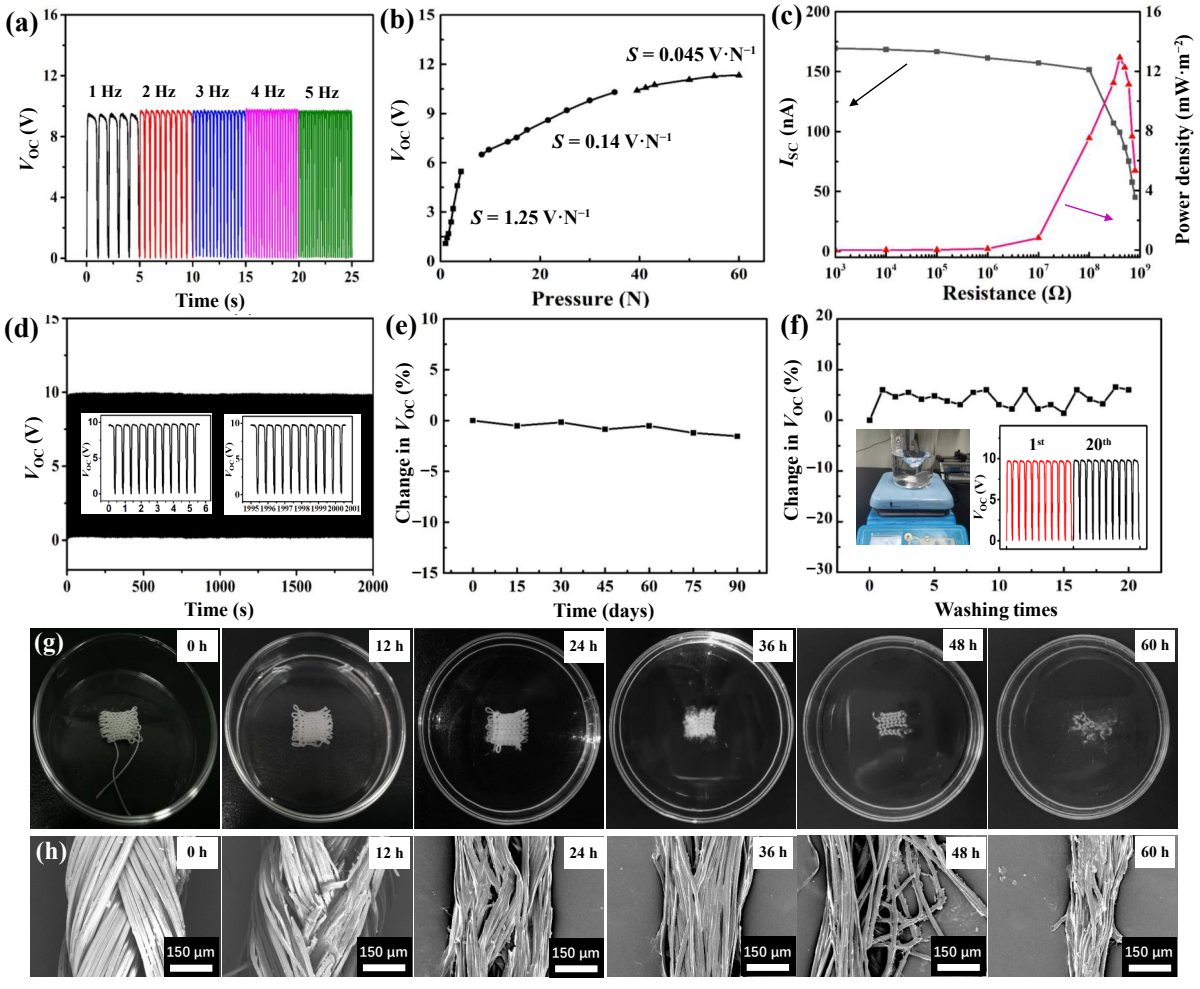

Figure 3 (a) The open-circuit voltage (V_{OC}) of the RC TENG-T (under the compressing force of 60 N and the frequency of 2 Hz). (b) The open-circuit voltage (V_{OC}) of the RC TENG-T under different external compressing force. (c) The variation of current and power density of the RC TENG-T measured with different external load resistances (under the compressing force of 60 N and the frequency of 2 Hz). (d) The stability test of the RC TENG-T under continuous impact for 4000 cycles (under the compressing force of 60 N and the frequency of 2 Hz). (e) The open-circuit voltage (V_{OC}) variation of the RC TENG-T in 90 days. (f) Washability test of the RC TENG-T (the insets exhibit the image of emulated laundering environment and the V_{OC} of RC TENG-T after first and 20 times washing). (g) Optical images of the RC TENG-T in the cellulase solution at different times during degradation. (h) SEM images of a RC-based composite yarn in RC TENG-T at different times during degradation.

tapping it for about 4000 cycles, and V_{OC} keeps stable around 10 V all the time (as shown in Fig. 3(d)). The insets exhibit the detailed V_{OC} for the early 10 cycles and the last 10 cycles, respectively, indicating that the RC TENG-T maintains an almost unchanged energy output under multiple compression. The result demonstrates the high stability and good durability of the RC TENG-T, which can be ascribed to the knit woven configuration stability of RC TENG-T under multiple compression. In addition, V_{OC} of RC TENG-T keeps unchanged after 90 days usage in the general mild environment (see Fig. 3(e)), indicating its long-term stability and durability in the normal application. Moreover, washability is also an essential basic requirement for the long-term usage of smart textiles. To demonstrate the washability of the RC TENG-T, a simulated domestic laundering environment is cultivated (as inset in Fig. 3(f)), the stirring speed is 500 rpm, and each washing process keeps 20 min. It can be seen from Fig. 3(f) that the energy harvesting capability of the RC TENG-T is well maintained after 20 times washing. Therefore, the RC TENG-T exhibits excellent washability, proving the formation of the strong bonds during the chemical modification of RC yarns. In the real application of textiles, the air permeability is one of the most important parameters reflecting their comfort [51]. The air permeability of the RC TENG-T is 1620 mm·s^{-1}, indicating its high wearing comfort, which should be attributed to its all-fiber structure without the use of any adhesion agent or dense film [52, 53]. Furthermore, as a type of TENG devices with vertical contact separation mode, the moisture resistance of the triboelectric materials is the most critical performance during the practical application of the RC TENG-T [16]. As shown in Fig. S8 in the ESM, the V_{OC} of the RC TENG-T is observed to be 8, 6.3, 3.2, 1.6, and 0.6 V at 60%, 70%, 80%, 90%, and 99% RH, respectively, indicating the significantly reduced output of the textile at high humidity levels (>80% RH). The inferior triboelectric performances of TENGs at high humidity level is commonly attributed to the water molecules adsorption effect of the triboelectric materials and the induced surface potential declining [54]. The enhanced surface hydrophobicity of the friction layers in RC TENG-T after chemical modification is conducive to the improvement of their moisture resistance [55], thus the RC TENG-T still presents an observable V_{OC} at even 99% RH.

Previous literatures have reported the biodegradability of bamboo viscose fibers in the cellulase solution, during which process the cellulose was degraded into glucose [56]. However, it is unclear whether the RC TENG-T with AgNPs densely wrapped

conductive core and the chemically modified surfaces can still be completely degraded. Hence, we investigate and evaluate the degradation experiments of RC TENG-T with enzymatic degradation method. Figure 3(g) shows the optical images of real-time degradation process every 12 h, indicating the complete degradation capability of RC TENG-T in cellulase solution. The RC-based composite yarns gradually unravel and fragmentize during the degradation process, in companied with the gradual decrease in their diameters (as shown in Fig. 3(h)). In addition, the weight change of RC TENG-T during degradation is recorded (as shown in Fig. S9 in the ESM). It can be seen that the mass of RC TENG-T is reduced by ≈ 50% within 24 h, and by ≈ 80% within 36 h, indicating that the degradation mainly occurs in the first 36 h. The weight loss reaches 100% after 72 h, indicating that RC TENG-T can be completely bio-degraded under the function of cellulase solution, which breaks down the β-1,4 glycosidic bond in RC yarn. It is worth noting that AgNPs cannot be degraded in cellulase solution, which can be recovered after simple filtration and drying.

The all-fiber structure of RC TENG-T gives it a unique advantage in wearable devices as power sources or self-powered sensors. As shown in Fig. 4(a), the RC TENG-T is integrated with clothes at the underarm position, and connected with a commercial capacitor (10 μF) to form a self-charging power system, where the rectifier converts the alternating current (AC) output to a direct current (DC) output (Fig. 4(b)). The capacitor can be charged to 2 V in around 100 s and then drives an electronic watch for around 20 s under the arm swing frequency of 1 Hz (Fig. 4(c)), indicating the energy harvesting and supplying capability of RC TENG-T during the wearer's exercise (as shown in Movie S1 in the ESM). In this experiment, the process of charging and powering is repeated three times, demonstrating the stability and durability of the RC TENG-T for driving wearable electronics. In addition, the RC TENG-T can be utilized as a wearable self-powered sensor for body motions detection. Figures 4(d)–4(f) show the voltage signal curves detected by the RC TENG-T integrated onto the heel, finger joint, and arm. Figure 4(d) shows the V_{OC} signals of the RC TENG-T sewn on the heel of a sock while detecting the steps of the tester. The RC TENG-T generates periodic electrical signals while the feet contacts and separates with the ground during the walking or running of the tester, thus recording the number of steps. The corresponding V_{OC} is around 6.5 V during the walking of the tester, while the V_{OC} reaches 10 V when the tester starts running, which should be attributed to the higher forces applied upon the RC TENG-T during running. In addition, the RC TENG-T was attached onto a finger to detect the bending of joint (Fig. 4(e)). The corresponding V_{OC} shows a linear increase with the increased bending degree of

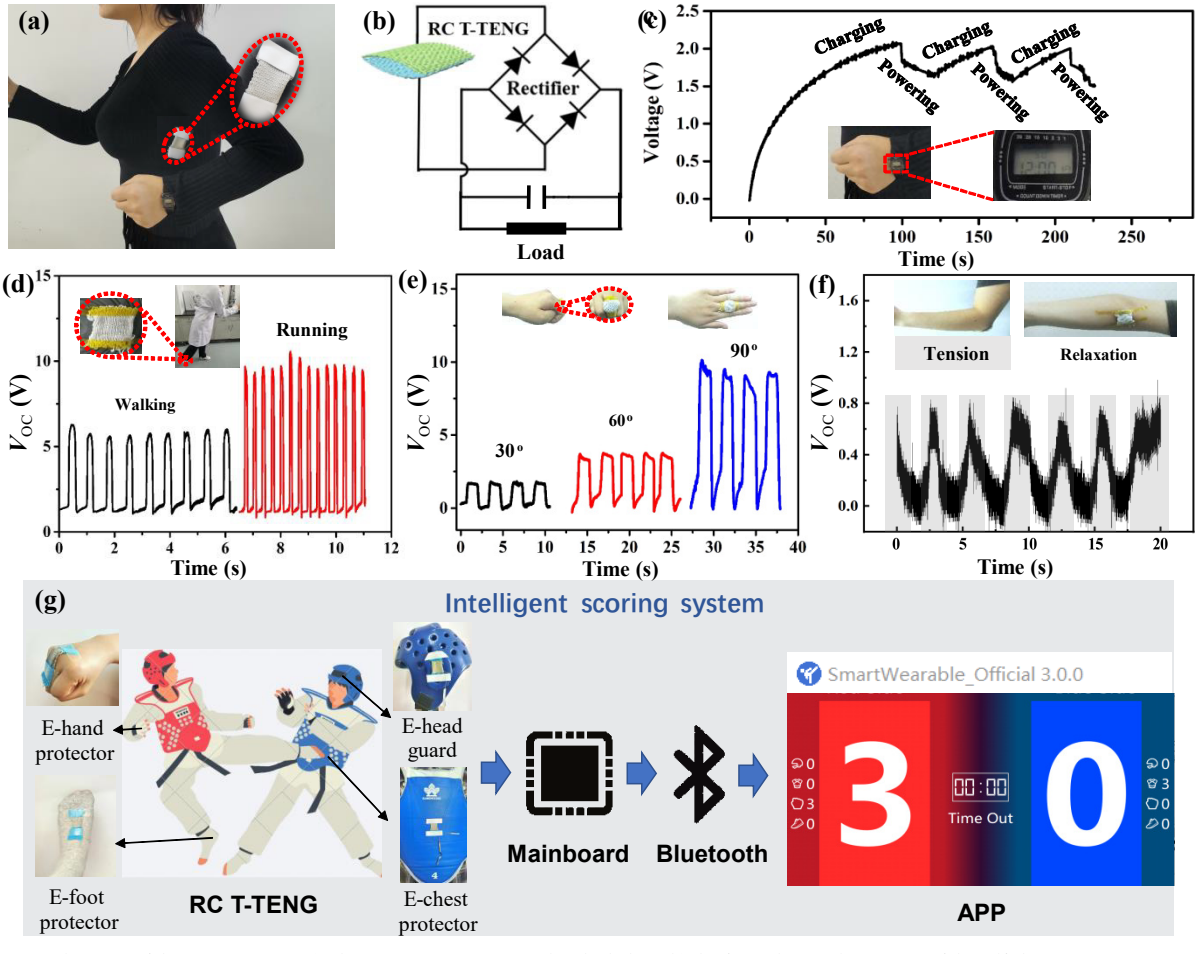

Figure 4 Applications of the RC TENG-T. (a) The RC TENG-T integrated with clothes, (b) the formed equivalent circuit of the self-charging power system, and its (c) charging voltage curve during energy collection and electronic watch driving by swing arm. The inserted photo shows an electronic watch driven by the RC TENG-T. (d) Voltage signals of the RC TENG-T-based sensor integrated onto the heel during the tester's walking and running monitoring. (e) Voltage signals of the RC TENG-T-based sensor integrated onto the finger joint under different bending angles. (f) Voltage signals of the RC TENG-T-based sensor integrated onto the arm under muscle tension and relaxation. (g) The intelligent Taekwondo scoring system based on the RC TENG-T.

the finger, indicating the accurate and quantitative human activities monitoring capability of RC TENG-T. Meanwhile, the V_{OC} signals of the RC TENG-T show excellent repeatability at the same bending degree, demonstrating the stable electrical output performance of the textile while monitoring the large human movements. The RC TENG-T attached onto the arm output obvious triboelectric signals by stressing the muscle, indicating that the tiny motions of muscles could also be monitored during its tension and relaxation processes (Fig. 4(f)).

Taking advantage of the self-powered pressure sensing ability of RC TENG-T, we construct an intelligent scoring system, which can improve the fairness of scoring in the Taekwondo competition. Compared with the regular pressure sensing chips used in the E-protector of Taekwondo, the RC TENG-T exhibits advantages including high durability, high response speed, and excellent replaceability, thus it shows great application potential to replace the traditional pressure sensing chips in the E-protector. The electric signals produced by RC TENG-T upon pressure can be received and transformed to the "scoring" directives by the signal processing and transmission module in the intelligent directive system, thus controlling the score change on the electronic screen (see Fig. 4(g)). The score only increases when the RC TENG-Ts on the attacker's E-protector and the opponent's E-protector both output signals, indicating a valid attack. In addition, different points can be added when the RC TENG-Ts on different positions output the signals, indicating the attack style recognition capability of the scoring system based on RC TENG-T (see Movie S2 in the ESM).

4 Conclusion

In summary, we present a strategy for material processing, characterization, performances optimization, and the derivated electronic device fabrication of an all-cellulose triboelectric textile (RC TENG-T) with excellent comprehensive performances, including good energy harvesting ability, long-term durability and washability, high comfortability, and complete biodegradability. The results show that the triboelectric output can be significantly improved via facile and straightforward chemical modification of two friction layers in this RC TENG-T, and the V_{OC} and I_{SC} are enhanced to 9.8 V and 160 nA, respectively. In addition, the RC TENG-T can be completely bio-degraded under the function of cellulase after 72 h, endowing it with wide application potential in the eco-friendly smart wearable devices including power source and self-powered sensors.

Electronic Supplementary Material: Supplementary material (SEM images and conductivity of AgNPs-coated RC yarn, effect of dopamine in the fabrication of AgNPs-coated RC yarn, XRD analysis of the RC yarns before and after chemical modification, contact angles of the RC TENG textiles before and after chemical modification, working principle of the RC TENG-T, ISC and QSC of the RC TENG-T, effect of humidity on the triboelectric output of the RC TENG-T, loss weight-time curve of the RC TENG-T during degradation) is available in the online version of this article at https://doi.org/10.26599/NRE.2024.9120139.

Acknowledgements

This work was supported by the Natural Science Foundation of Beijing Municipality (2232049), Young Elite Scientist Sponsorship Program by BAST (BYESS2022211), and the Beijing Outstanding Young Talents (BPHR202203066). The Classified Development of Municipal Colleges-the Project of Constructing the Emerging Interdisciplinary Platform Based on "Clothing Science" of Beijing Institute of Fashion Technology (11000024T000003073871) and the Beijing Scholar Program (RCQJ20303) should also be acknowledged.

Declaration of conflicting interests

The authors declare no conflicting interests regarding the content of this article.

Data availability

All data needed to support the conclusions in the paper are presented in the manuscript and/or the Supplementary Materials. Additional data related to this paper may be requested from the corresponding author upon request.

Author contributions

Q. Lian, J. Li, Y. Liang, and T. Li performed the experiments and analyzed the data, Q. Li and R. Wang supervised parts of the experiments, H. G. Wu proposed this project, provided financial support, supervised the experiments, and conducted the revision of the manuscript. All authors have given approval to the final version of the manuscript.

References

[1] Sharma, S.; Pradhan, G. B.; Jeong, S.; Zhang, S. P.; Song, H.; Park, J. Y. Stretchable and all-directional strain-insensitive electronic glove for robotic skins and human-machine interfacing. *ACS Nano* **2023**, *17*, 8355–8366.

[2] Sun, F. Q.; Jiang, H.; Wang, H. Y.; Zhong, Y. H.; Xu, Y. M.; Xing, Y.; Yu, M. H.; Feng, L. W.; Tang, Z.; Liu, J. et al. Soft fiber electronics based on semiconducting polymer. *Chem. Rev.* **2023**, *123*, 4693–4763.

[3] Ke, H. Z.; Gao, M. Y.; Li, S. M.; Qi, Q. C.; Zhao, W. C.; Li, X.; Li, S. S.; Kuvondikov, V.; Lv, P. F.; Wei, Q. F.; Ye, L. Advances and future prospects of wearable textile- and fiber-based solar cells. *Solar RRL* **2023**, *7*, 2300109.

[4] Qi, L. F.; Kong, L. J.; Wang, Y.; Song, J. H.; Azam, A.; Zhang, Z. T.; Yan, J. Y. Recent progress in application-oriented self-powered microelectronics. *Adv. Energy Mater.* **2023**, *13*, 2302699.

[5] Choi, D.; Lee, Y.; Lin, Z. H.; Cho, S.; Kim, M.; Ao, C. K.; Soh, S.; Sohn, C.; Jeong, C. K.; Lee, J. et al. Recent advances in triboelectric nanogenerators: From technological progress to commercial applications. *ACS Nano* **2023**, *17*, 11087–11219.

[6] Wang, W.; Yu, A. F.; Zhai, J. Y.; Wang, Z. L. Recent progress of functional fiber and textile triboelectric nanogenerators: Towards electricity power generation and intelligent sensing. *Adv. Fiber Mater.* **2021**, *3*, 394–412.

[7] Mathew, A. A.; Chandrasekhar, A.; Vivekanandan, S. A review on real-time implantable and wearable health monitoring sensors based on triboelectric nanogenerator approach. *Nano Energy* **2021**, *80*, 105566.

[8] Wang, Z. L. Triboelectric nanogenerator (TENG)-sparking an energy and sensor revolution. *Adv. Energy Mater.* **2020**, *10*, 2000137.

[9] Zhu, P. H.; Ullah, Z.; Zheng, S. R.; Yang, Z. R.; Yu, S. W.; Zhu, S. P.; Liu, L. W.; He, A. H.; Wang, C. G.; Li, Q. Ultrahigh current output from triboelectric nanogenerators based on UIO-66 materials for electrochemical cathodic protection. *Nano Energy* **2023**, *108*, 108195.

[10] Zhao, D. Z.; Zhang, K. J.; Meng, Y.; Li, Z. Y.; Pi, Y. C.; Shi, Y. J.; You, J. C.; Wang, R. K.; Dai, Z. Y.; Zhou, B. P. et al. Untethered

triboelectric patch for wearable smart sensing and energy harvesting. *Nano Energy* **2022**, *100*, 107500.
[11] Liu, S. L.; Tong, W. S.; Gao, C. X.; Liu, Y. L.; Li, X. N.; Zhang, Y. H. Environmentally friendly natural materials for triboelectric nanogenerators: A review. *J. Mater. Chem. A* **2023**, *11*, 9270–9299.
[12] Du, T. L.; Chen, Z. X.; Dong, F. Y.; Cai, H.; Zou, Y. J.; Zhang, Y. W.; Sun, P. T.; Xu, M. Y. Advances in green triboelectric nanogenerators. *Adv. Funct. Mater.* **2024**, *34*, 2313794.
[13] Wei, Z. T.; Wang, J. L.; Liu, Y. H.; Yuan, J. X.; Liu, T.; Du, G. L.; Zhu, S. Q. Y.; Nie, S. X. Sustainable triboelectric materials for smart active sensing systems. *Adv. Funct. Mater.* **2022**, *32*, 2208277.
[14] Meng, X. J.; Cai, C. C.; Luo, B.; Liu, T.; Shao, Y. Z.; Wang, S. F.; Nie, S. X. Rational design of cellulosic triboelectric materials for self-powered wearable electronics. *Nano-Micro Lett.* **2023**, *15*, 124.
[15] Du, G. L.; Wang, J. L.; Liu, Y. H.; Yuan, J. X.; Liu, T.; Cai, C. C.; Luo, B.; Zhu, S.; Wei, Z. Y.; Wang, S. Q. Y. et al. Fabrication of advanced cellulosic triboelectric materials via dielectric modulation. *Adv. Sci.* **2023**, *10*, 2206243.
[16] Shao, Y. Z.; Luo, B.; Liu, T.; Cai, C. C.; Meng, X. J.; Wang, S. F.; Nie, S. X. Harvesting energy from extreme environmental conditions with cellulosic triboelectric materials. *Mater. Today* **2023**, *66*, 348–370.
[17] Chen, J.; Guo, H. Y.; Pu, X. J.; Wang, X.; Xi, Y.; Hu, C. G. Traditional weaving craft for one-piece self-charging power textile for wearable electronics. *Nano Energy* **2018**, *50*, 536–543.
[18] Mule, A. R.; Dudem, B.; Patnam, H.; Graham, S. A.; Yu, J. S. Wearable single-electrode-mode triboelectric nanogenerator via conductive polymer-coated textiles for self-power electronics. *ACS Sustain. Chem. Eng.* **2019**, *7*, 16450–16458.
[19] Yu, Z. C.; Zhu, Z. Y.; Wang, Y. S.; Wang, J. F.; Zhao, Y. H.; Zhang, J. L.; Qin, Y.; Jiang, Q.; He, H. J. Wearable cotton fabric-based single-electrode-mode triboelectric nanogenerator for self-powered human motion monitoring. *Cellulose* **2023**, *30*, 5355–5371.
[20] Yang, M. Y.; Tian, X.; Hua, T. Green and recyclable cellulose based TENG for sustainable energy and human-machine interactive system. *Chem. Eng. J.* **2022**, *442*, 136150.
[21] Yan, J.; Lv, M. D.; Qin, Y. B.; Wang, B. J.; Kang, W. M.; Li, Y. F.; Yang, G. Triboelectric nanogenerators based on membranes comprised of polyurethane fibers loaded with ethyl cellulose and barium titanate nanoparticles. *ACS Appl. Nano Mater.* **2023**, *6*, 5675–5684.
[22] Yu, Z. C.; Zhu, Z. Y.; Zhang, Y. Z.; Li, X. Q.; Liu, X.; Qin, Y.; Zheng, Z. R.; Zhang, L. Y.; He, H. L. Biodegradable and flame-retardant cellulose-based wearable triboelectric nanogenerator for mechanical energy harvesting in firefighting clothing. *Carbohydr. Polym.* **2024**, *334*, 122040.
[23] Xu, S. H.; Zhao, H. Q.; Li, Q.; Zhang, R. Y.; Gao, S.; Wang, F.; Li, G. L.; Chen, B. L.; Yu, H. P.; Liu, S. X. et al. Multi-dimensional, transparent and foldable cellulose-based triboelectric nanogenerator for touching password recognition. *Nano Energy* **2022**, *98*, 107307.
[24] Song, J. M.; Latif, M.; Jiang, Y. X. Z.; Ounaies, Z.; Kim, J. High-performance flexible triboelectric nanogenerator based on micropatterned allicin-grafted cellulose film. *Mater. Today Nano* **2024**, *26*, 100475.
[25] Bai, Z. Q.; Xu, Y. L.; Zhang, Z.; Zhu, J. J.; Gao, C.; Zhang, Y.; Jia, H.; Guo, J. S. Highly flexible, porous electroactive biocomposite as attractive tribopositive material for advancing high-performance triboelectric nanogenerator. *Nano Energy* **2020**, *75*, 104884.
[26] Huang, J. Q.; Zhang, Y.; Yu, H. J.; Han, G. P.; Cheng, W. L. Cellulose-based triboelectric nanogenerator prepared by multi-fluid electrospinning for respiratory protection and self-powered sensing. *Actuators* **2024**, *13*, 178.
[27] Zhang, L.; Liao, Y.; Wang, Y. C.; Zhang, S.; Yang, W. Q.; Pan, X. J.; Wang, Z. L. Cellulose II aerogel-based triboelectric nanogenerator. *Adv. Funct. Mater.* **2020**, *30*, 2001763.
[28] Bai, Z. Q.; Xu, Y. L.; Li, J. C.; Zhu, J. J.; Gao, C.; Zhang, Y.; Wang, J.; Guo, J. S. An eco-friendly porous nanocomposite fabric-based triboelectric nanogenerator for efficient energy harvesting and motion sensing. *ACS Appl. Mater. Interfaces* **2020**, *12*, 42880–42890.
[29] Huang, J. Y.; Hao, Y.; Zhao, M.; Li, W.; Huang, F. L.; Wei, Q. F. All-fiber-structured triboelectric nanogenerator via one-pot electrospinning for self-powered wearable sensors. *ACS Appl. Mater. Interfaces* **2021**, *13*, 24774–24784.
[30] Zhang, R. Y.; Dahlström, C.; Zou, H. Y.; Jonzon, J.; Hummelgård, M.; Örtegren, J.; Blomquist, N.; Yang, Y.; Andersson, H.; Olsen, M. et al. Cellulose-based fully green triboelectric nanogenerators with output power density of 300 W·m^{-2}. *Adv. Mater.* **2020**, *32*, 2002824.
[31] Zhang, J. T.; Hu, S. M.; Shi, Z. J.; Wang, Y. F.; Lei, Y. Q.; Han, J.; Xiong, Y.; Sun, J.; Zheng, L.; Sun, Q. et al. Eco-friendly and recyclable all cellulose triboelectric nanogenerator and self-powered interactive interface. *Nano Energy* **2021**, *89*, 106354.
[32] Lou, M. N.; Abdalla, I.; Zhu, M. M.; Yu, J. Y.; Li, Z. L.; Ding, B. Hierarchically rough structured and self-powered pressure sensor textile for motion sensing and pulse monitoring. *ACS Appl. Mater. Interfaces* **2020**, *12*, 1597–1605.
[33] Lu, C. W.; Wang, X. Y.; Shen, Y.; Xu, S. J.; Huang, C. X.; Wang, C. P.; Xie, H. J.; Wang, J. F.; Yong, Q.; Chu, F. X. Skin-like transparent, high resilience, low hysteresis, fatigue-resistant cellulose-based eutectogel for self-powered e-skin and human-machine interaction. *Adv. Funct. Mater.* **2023**, *34*, 2311502.
[34] Wang, T.; Li, S. Y.; Tao, X. L.; Yan, Q.; Wang, X. L.; Chen, Y.; Huang, F. J.; Li, H. X.; Chen, X. Y.; Bian, Z. F. Fully biodegradable water-soluble triboelectric nanogenerator for human physiological monitoring. *Nano Energy* **2022**, *93*, 106787.
[35] Wang, R.; Ma, J. M.; Ma, S.; Zhang, Q. R.; Li, N.; Ji, M. M.; Jiao, T. F.; Cao, X. A biodegradable cellulose-based flame-retardant triboelectric nanogenerator for fire warning. *Chem. Eng. J.* **2022**, *450*, 137985.
[36] Yang, B.; Xiong, Y.; Ma, K.; Liu, S. R.; Tao, X. M. Recent advances in wearable textile-based triboelectric generator systems for energy harvesting from human motion. *EcoMat* **2020**, *2*, e12054.
[37] Dong, K.; Peng, X.; Wang, Z. L. Fiber/fabric-based piezoelectric and triboelectric nanogenerators for flexible/stretchable and wearable electronics and artificial intelligence. *Adv. Mater.* **2020**, *32*, 1902549.
[38] Cui, X. J.; Li, A.; Zheng, Z. N.; Wu, H. G.; Wang, R. A machine-braided flame-retardant triboelectric yarn/textile for fireproof application. *Adv. Mater. Technol.* **2023**, *8*, 2202116.
[39] Nie, S. X.; Fu, Q.; Lin, X. J.; Zhang, C. Y.; Lu, Y. X.; Wang, S. F. Enhanced performance of a cellulose nanofibrils-based triboelectric nanogenerator by tuning the surface polarizability and hydrophobicity. *Chem. Eng. J.* **2021**, *404*, 126512.
[40] Nie, S. X.; Cai, C. C.; Lin, X. J.; Zhang, C. Y.; Lu, Y. X.; Mo, J. L.; Wang, S. F. Chemically functionalized cellulose nanofibrils for improving triboelectric charge density of a triboelectric nanogenerator. *ACS Sustain. Chem. Eng.* **2020**, *8*, 18678–18685.
[41] Dong, K.; Deng, J. N.; Zi, Y. L.; Wang, Y. C.; Xu, C.; Zou, H. Y.; Ding, W. B.; Dai, Y. J.; Gu, B. H.; Sun, B. Z. et al. 3D orthogonal woven triboelectric nanogenerator for effective biomechanical energy harvesting and as self-powered active motion sensors. *Adv. Mater.* **2017**, *29*, 1702648.
[42] Wang, J.; Li, X. H.; Zi, Y. L.; Wang, S. H.; Li, Z. L.; Zheng, L.; Yi, F.; Li, S. M.; Wang, Z. L. A flexible fiber-based supercapacitor-triboelectric-nanogenerator power system for wearable electronics. *Adv. Mater.* **2015**, *27*, 4830–4836.
[43] Oun, A. A.; Rhim, J. W. Preparation and characterization of sodium carboxymethyl cellulose/cotton linter cellulose nanofibril composite films. *Carbohyd. Polym.* **2015**, *127*, 101–109.
[44] Yang, Y.; Zhang, H. L.; Chen, J.; Lee, S.; Hou, T. C.; Wang, Z. L. Simultaneously harvesting mechanical and chemical energies by a hybrid cell for self-powered biosensors and personal electronics. *Energy Environ. Sci.* **2013**, *6*, 1744–1749.
[45] Ma, R. J.; Kang, B.; Cho, S.; Choi, M.; Baik, S. Extraordinarily high conductivity of stretchable fibers of polyurethane and silver nanoflowers. *ACS Nano* **2015**, *9*, 10876–10886.
[46] Du, D. H.; Li, P. C.; Ouyang, J. Y. Graphene coated nonwoven fabrics as wearable sensors. *J. Mater. Chem. C* **2016**, *4*, 3224–3230.

[47] Xu, C.; Zi, Y. L.; Wang, A. C.; Zou, H. Y.; Dai, Y. J.; He, X.; Wang, P. H.; Wang, Y. C.; Feng, P. Z.; Li, D. W. et al. On the electron-transfer mechanism in the contact-electrification effect. *Adv. Mater.* **2018**, *30*, 1706790.
[48] Wu, Y. X.; Cui, X. J.; Wu, H. G.; Su, Z. Q. All-polymeric fibrous triboelectric nanogenerator for self-powered intelligent active motions monitoring system. *Chem. Eng. J.* **2023**, *469*, 143708.
[49] Fu, K.; Zhou, J.; Wu, H. G.; Su, Z. Q. Fibrous self-powered sensor with high stretchability for physiological information monitoring. *Nano Energy* **2021**, *88*, 106258.
[50] Lee, H. J.; Chun, K. Y.; Oh, J. H.; Han, C. S. Wearable triboelectric strain-insensitive pressure sensors based on hierarchical superposition patterns. *ACS Sens.* **2021**, *6*, 2411–2418.
[51] Jahan, I.; Moiz, A.; Wang, X. Creating an interconnected PVA nanofibrous membrane on cotton fabrics by dip-coating of PDMS-TMS for versatile protection without compromising comfort. *Cellulose* **2019**, *26*, 8179–8190.
[52] Guo, Y. B.; Zhang, X. S.; Wang, Y.; Gong, W.; Zhang, Q. H.; Wang, H. Z.; Brugger, J. All-fiber hybrid piezoelectric-enhanced triboelectric nanogenerator for wearable gesture monitoring. *Nano Energy* **2018**, *48*, 152–160.
[53] Ye, X. R.; Shi, B. H.; Li, M.; Fan, Q.; Qi, X. J.; Liu, X. H.; Zhao, S. K.; Jiang, L.; Zhang, X. J.; Fu, K. et al. All-textile sensors for boxing punch force and velocity detection. *Nano Energy* **2022**, *97*, 107114.
[54] Cai, C. C.; Liu, Y. H.; Li, L. C.; Dong, T. T.; Chen, W.; Zhou, Z.; Li, Q. X.; Sun, Y.; Peng, W. X.; Wang, J. L. et al. Wet-resistant, dustproof, and germproof self-powered lignocellulosic triboelectric filters for respiratory protection, monitoring, and diagnosis. *Chem. Eng. J.* **2023**, *476*, 146819.
[55] Jiang, C. M.; Li, X. J.; Ying, Y. B.; Ping, J. F. A multifunctional TENG yarn integrated into agrotextile for building intelligent agriculture. *Nano Energy* **2020**, *74*, 104863.
[56] Chu, F. J.; Lin, C. W.; I, Y. P.; Wu, C. H.; Chen, D. H. Hydrolysis of bamboo cellulose and cellulase characteristics by *Streptomyces griseoaurantiacus* ZQBC691. *J. Taiwan Inst. Chem. Eng.* **2012**, *43*, 220–225.

Qiru Lian received her Bachelor of Science degree from Department of Applied Chemistry in Qiqihar University in 2021 and her Master degree from Department of Material Science and Technology, Beijing Institute of Fashion Technology in 2023 (supervised by Prof. Hanguang Wu). Her research interest focused on the development of cellulose-based triboelectric nanogenerators and their applications in energy harvesting.

Jiaxin Li received her Bachelor degree for Department of Polymer Materials and Engineering in Beijing Institute of Fashion Technology in 2023.

Ting Li received her Bachelor's degree from Chemical Engineering, Liaoning University of Technology in 2022. She is currently a graduate student in Department of Material Science and Technology, Beijing Institute of Fashion Technology (supervised by Prof. Hanguang Wu). Her current research focuses on the smart wearable pressure-sensing textile.

Qiuyu Li received her Bachelor's degree in Zhejiang University of Science and Technology in 1999. She joined the faculty of the Department of Material Science and Technology, Beijing Institute of Fashion Technology in 2003, and received her Master's degree in Beijing Institute of Fashion Technology in 2015. Her research interests focus on Textile Materials and Textile Design.

Yifang Liang received her Bachelor of Engineering degree from the Department of Polymer Materials and Engineering in Soochow University in 2023. She is currently a graduate student in Department of Material Science and Technology, Beijing Institute of Fashion Technology (supervised by Prof. Hanguang Wu). Her research interests focus on the smart wearable materials and functional textiles.

Hanguang Wu received her Bachelor of Engineering degree from the Department of Polymer Science and Technology in Beijing University of Chemical Engineering in 2010, and her Ph.D. degree from the Department of Polymer Science and Technology in Beijing University of Chemical Engineering in 2016 (under the supervision of Prof. Ming Tian). She did her postdoctoral research at the Chemistry Department of Tsinghua University, with Prof. Gaoquan Shi. She joined the faculty of the Department of Material Science and Technology, Beijing Institute of Fashion Technology in 2018. Her research interests focus on the development of the functional polymers and smart wearable materials.

Rui Wang is currently a professor at Beijing Institute of Fashion Technology and part-time professor and doctoral supervisor at Sichuan University and Tianjin Polytechnic University. Her research interests focus on the preparation and performance optimization of composite functional fibers and smart wearable materials.